A contribution to late Middle Paleolithic chronology of the Levant: New luminescence ages for the Atlit Railway Bridge site, Coastal Plain, Israel

Porat, N. ; Jain, Mayank; Ronen, A.; Horwitz, L.K.

Published in:
Quaternary International

Link to article, DOI:
10.1016/j.quaint.2017.06.017

Publication date:
2018

Document Version
Peer reviewed version

A contribution to late Middle Paleolithic chronology of the Levant: New luminescence ages for the Atlit Railway Bridge site, Coastal Plain, Israel

N. Porat[(1)], M. Jain[(2)], A. Ronen[(3)], L.K. Horwitz[(4)].

(1) The Geological Survey of Israel, 30 Malkhe Israel St., Jerusalem 95501, Israel
(2) Radiation Research Division, Risø National Laboratory, Technical University of Denmark (Risø DTU), DK-4000 Roskilde, Denmark
(3) Zinman Institute of Archaeology, University of Haifa, Haifa 31905, Israel
(4) Natural History Collections, Faculty of Life Sciences, The Hebrew University, Jerusalem 91904, Israel

Abstract

The Atlit Railway Bridge (ARB) prehistoric site is located on the northern coastal plain of Israel, within natural caves which formed within calcareous aeolianites (kurkar), perhaps during a high sea-stand. Flint artifacts and faunal remains were found embedded in the kurkar infill of two caves, and the artifacts belong to the Levantine later Mousterian tradition. The aeolianites in which the caves had developed were previously constrained by $IRSL_{50}$ dating of feldspars to be older than the last interglacial highest sea-stand (Frechen M. et al. 2004; Chronology of Pleistocene sedimentary cycles in the Carmel Coastal Plain of Israel. Quaternary International 121, 1-52), providing a maximum age for the artifacts.

Samples for luminescence dating were collected from the infill of the two caves (II and III), from the same deposits as the archaeological finds. Both quartz and alkali feldspars (KF) were extracted and measured using four different luminescence signals: optically stimulated luminescence (blue OSL) and violet stimulated luminescence (VSL) on quartz; and the infrared stimulated luminescence (IRSL) post-IR-IR_{290} signal and the IR_{50} signal corrected for anomalous fading on KF.

The ages obtained from analyses of the different minerals and signals mostly agree within errors. The new luminescence ages date the sediment infill in Caves III and II to ~90 ka and ~70 ka, respectively, indicating that hominin occupation of this locality is coeval with the nearby Skhul Cave and Layer B in Tabun Cave.

Key Words

Blue OSL, VSL, IRSL, MIS 5, beachrock, eastern Mediterranean coast, Mousterian

Introduction

The southern Levant is a critical region for examining hominin biological and cultural evolution during the Middle Paleolithic (MP), particularly given the presence of both Neanderthals and early anatomically modern humans in the region (McCown and Keith, 1939; Rak, 1998; Shea, 2010; Weinstein-Evron, 2015; Langdon, 2016). Moreover, lithic typologies attest to extensive inter-site variability during this period, but the factors responsible - different hominin abilities, socio-cultural choice and behaviours, climatic and local ecological factors, or chronology - are unclear (e.g. Jelinek, 1981; Bar-Yosef and Meignen, 1992; Goren-Inbar and Belfer-Cohen, 1998; Hovers, 2009; Belfer-Cohen and Hovers, 2010; Kadowaki, 2013). Finally, the timing and nature of the transition between the late MP and the Upper Paleolithic is of special interest, especially given the debate over cultural continuity and apparent association of this period with the dispersal of anatomically modern humans Out of Africa (Bar Yosef, 2002; Shea, 2008; Belfer-Cohen and Goring-Morris, 2009; Hershkovitz et al. 2015). Consequently, dating MP sites is a critical issue.

Initially, radiocarbon was the principal source of chronometric data for the MP (e.g. Weinstein, 1984; Henry, 1992).Advances in this field of dating – including introduction of accelerator mass spectrometry, improved pretreatment chemistry of samples as well as statistical tools – still renders radiocarbon an essential tool for dating terminal MP sites (e.g. Bronk Ramsey et al., 2004; Bronk Ramsey, 2009; Taylor and Bar-Yosef, 2016). However additional radiometric methods are needed to date deposits and sites from early and middle MP which are beyond the limit of radiocarbon (ca. 40-60,000 years BP, Taylor and Bar-Yosef, 2016:24). Methods commonly applied to MP occupations include electron spin resonance (ESR) for teeth (see review by Grün, 2006), and luminescence dating methods which include among other techniques thermoluminescence (TL) for burnt flints (e.g. Valladas et al., 2013) and optical stimulated luminesce (OSL) for quartz grains in sediments (see review by Roberts et al., 2015). They have extended the range of dating for the MP considerably and improved precision of dating through cross-checking of ages between different methods to create a more robust chronometric framework for this period in the southern Levant (e.g. Mercier et al., 2013). The luminescence methods have proved especially useful, given

that many sites lack organic remains (bones, teeth, charcoal) and contain only burnt flint and sediment.

As new techniques are developed in luminescence dating, there is a need to test them in sites where they can be compared to well-established methods such as radiocarbon or OSL (Wintle, 2008). Some of the new methods, such as violet stimulated luminescence (VSL; Jain, 2009), aim at dating samples older than 200 ka, a time range usually not covered by OSL. The best test case for a comparative study of luminescence methods is a site which is younger than 200 ka, is rich in both quartz and feldspars, and has some age control. Atlit Railway Bridge (ARB) is such a site; its relative age has been established by previous luminescence dating to be younger than the last interglacial high sea-stand (MIS 5e; Frechen et al., 2004); according to the lithic assemblage it is of late Mousterian age (Ronen et al., 2008); and it is situated in the coastal plain sandy aeolianites and soil sequence rich in quartz and feldspars.

Here we present a comparison of several luminescence methods on samples from ARB, show how the ages compare with each other, and provide a robust age for the site. These ages are then placed within the context of late MP chronology for the southern Levant.

Background to the Study Region

Mount Carmel and the adjacent coastal plain of northern Israel (Fig. 1) are characterized by a Mediterranean climate with a mean annual temperature of 19 ºC and annual precipitation of ca. 600-800 mm. Varied habitats are available in this region, ranging from typical Mediterranean forests or maquis on Mount Carmel to dunes, swamps and agricultural land on the coastal plain (Orni and Efrat, 1971). The region is of immense importance for prehistory, with well over 200 documented prehistoric sites spanning a range of periods and cultures in an area of ca. 30,000 ha (Olami, 1984; Ronen, 1977; Tsatskin and Ronen, 1999; Nadel et al., 2012; Weinstein-Evron, 2015). Of particular note are several caves and rock shelters clustered on the western side of Mount Carmel (Tabun, Jamal, Skhul, el Wad, Sefunim, Kebara and Misliya), as well as other sites in northern Israel (Qafzeh, Amud, Manot) that have yielded a rich and lengthy record of archaeological remains dating to the Lower Paleolithic (Late Acheulian and Acheulo-Yabrudian cultural entities, ca. 500-220 ka) and Middle Paleolithic (Mousterian cultural entities, ca. 245-45 to 47 ka) (Garrod and Bate, 1937; Ronen, 1984; Weinstein-Evron et

al., 2003; Bar-Yosef and Meignen, 2007; Shea, 2013; Hershkovitz et al., 2015; Weinstein-Evron 2015). The MP sites are unparalleled in that they contain remains of both early anatomically modern humans (Skhul I-IX, Tabun C2, Manot; Qafzeh) and Neanderthals (Kebara 1-2, Tabun C1, Tabun B, Geula, Amud), making the Carmel in particular, and northern Israel in general, a unique region for the study of human evolution (e.g. McCown and Keith, 1939; papers in Akazawa et al., 1998; papers in Bar-Yosef and Pilbeam, 2000; Shea, 2010; Langdon, 2016).

Mousterian sites on the adjacent Carmel narrow coastal plain are, in contrast, ephemeral and comprise scanty cultural and organic remains embedded in aeolian calcarenite or red soils, locally termed kurkar and hamra, respectively (e.g. Ronen, 1977; Ronen et al., 1999; Galili et al., 2007; Ronen and Chernikov, 2010; Galili et al, this volume). One such occurrence is the Atlit Railway Bridge (ARB) locality, situated ca. 5 km northwest of the caves of Tabun and Skhul (Fig. 1; Ronen et al., 2007).

The topography of the Israeli coast is made up of four to five longitudinal Pleistocene kurkar ridges that run parallel (north-south) to the coast. These ridges alternate with troughs filled with clays, sands and alluvial sediments (Issar, 1968; Almagor, 2002; Frechen et al., 2004; Sivan and Porat, 2004). The ARB find locality, whose dating is the focus of this paper, lies in the third ridge from the west, commonly known as the "Carmel coast" or "Highway" ridge (Eytam and Ben-Avraham, 1992; Ronen et al., 2008).

Geological background

The “Highway” kurkar ridge adjacent to Atlit is composed of the following units, which were dated by Frechen et al. (2004) by $IRSL_{50}$ (from bottom to top; Fig. 2):

Unit 1: a basal indurated aeolianite dated to 153±31 ka.

Unit 2: a reddish loam.

Unit 3: beachrock composed of complete and large fragments of shells in a coarse sand matrix, of variable thickness, occurring at elevations ranging between +4 and +9 m asl. The presence of the fossil mollusk, *Persitistrombus latus* (formerly *Strombus bubonius* or *S. latus*), indicates a Last Interglacial age (MIS 5; Gignoux 1913). Using the elevation, the age of the unit can further be constrained to the peak of the last interglacial (MIS 5e; Galili et al., 2007).

Unit 4: cemented aeolianite dated to 143±27 ka.
Unit 5: a sandy reddish loam dated to 76±7 ka.
Unit 6: the latest aeolianite on the ridge dated to 60±17 ka.
Unit 7: a largely eroded sandy reddish loam dated to12±2 ka.
Three natural caves (I, II, III) were identified on the flanks of this kurkar ridge (Fig. 2; Frechen et al., 2004; Ronen and Chernikov, 2010). The caves open to both the eastern and western aspects of the ridge and Ronen et al. (2008) have suggested that they were perhaps formed following marine abrasion during a high stand of the sea. The cave infill comprises loosely cemented layer of finely crushed, tiny shell fragments disseminated in a coarse sand matrix. The densest concentration of cultural remains, i.e. indicating the most intensive hominin occupation, were found in the uppermost portion of the infill, with scant remains in the lower fill. The layer bearing the cultural deposit was covered by an unconsolidated fine, whiter sand ca. 5-20 cm thick, also containing rare fragments of shell. This layer has been interpreted as representing a retreat of the coast line (Ronen et al., 2008). The cultural deposit and overlying quartz sand layer in both caves were capped by large blocks of roof collapse (Fig. 3a).

Archaeological background

In 2002, collections were made of archaeological remains that had eroded out of the caves or were exposed in the cave fill (Ronen et al., 2008). The find location of all items collected was noted and the stratigraphy of the infill documented (Fig. 3). The fill of Cave I appears to be archaeologically sterile and cultural remains were found only in the eastern entrances of Caves II and III. At this time, samples were collected from the archaeological units of Cave II and III for luminescence dating.

Cave II: The cave entrance is 7.7 m wide and 5m high. A narrow chimney (0.5 m diameter), located adjacent to the south wall of the cave, leads to the base of the red loam (Unit II) some 2.6 m up (Fig. 3b). The Unit III deposit is ca. 2 m thick and contains two hearths (H1 and H2), lithic tools and fauna. The hearths were visible in the sections and were characterized by dark, well constrained lenses. H1 was black, while the upper part of H2 was black while the lower part was pinkish in color. H1 was ~30 cm in length and 5 cm thick and lay at the top of the cultural layer, while H2 was ~50 cm in length and 8 cm thick, and lay at a lower elevation within this deposit (Fig. 5 in Ronen et al., 2008). Both hearths were surrounded by lithic artifacts and flakes, with one burnt flake each,

respectively. In the vicinity of H1 there was a poorly preserved long bone shaft fragment and a small fragment of ostrich eggshell, while isolated fragments of animal bone were found around H2. This unit is covered by a layer of unconsolidated fine white sand overlain by small aeolianite debris and large blocks of roof collapse.

Cave III: The cave entrance is 7.3 m wide and 1.7 m high (Fig. 3c). Several concentrations of relatively well preserved animal bones and a tooth were found intermingled with lithic artefacts. Seashells were found mainly close to the surface of the cultural deposit, while one shell and a flake were found in the middle of the infill. Unconsolidated white sand was deposited above the beachrock and the whole infill was sealed by huge blocks from the collapsed cave roof.

Lithic assemblage: A small lithic assemblage of ca. 20 items was recovered from the ARB caves, mostly derived from Cave II. The lithic assemblage was manufactured on high quality brown Mount Carmel flint. Both artefacts and flakes are fresh and were found horizontally aligned in the deposit. The use of Levallois technique clearly predominates with dihedral, faceted or 'chapeau-de-gendarme' flake butts. No cores were found and most artefacts were complete. Two retouched tools were found (a straight side-scraper, a backed knife; Fig. 5) as well as several lightly retouched/used pieces (e.g. Ronen 2008: Fig 7, items 4 and 7). When present, retouch was generally light (Ronen et al. 2008).

The artifacts show features comparable with those from both Layers B and C of nearby Tabun Cave (attributed to the Middle and Late Mousterian, respectively) and Skhul Layer B (Jelinek, 1982; Ronen et al., 2008; Shea, 2010, 2013; Culley et al., 2013). The ARB finds also resemble other late Mousterian lithic assemblages recovered in the red loam (Hamra) deposits along the Carmel coast (Issar and Kafri, 1969; Ronen, 1977, 1983; 1994; Tsatskin and Ronen, 1999; Galili et al., 2007; Ronen and Chernikov, 2010). The absence of abrasion on the ARB tools and their horizontal position in the deposit suggest that the artefacts are in primary position, with little or no disturbance.

Faunal assemblage: Fauna are not preserved in the red loam Mousterian find localities along the Israeli Mediterranean coast (Ronen and Chernikov, 2010). They are however, preserved at the ARB site, and in four other find spots within kurkar on the Carmel and Galilee coasts (Galili et al., 2007).

The majority of faunal remains from ARB that could be identified to taxon were recovered from Cave III (Fig. 4; Table 1). The range of species identified resembles that found in other Mousterian sites in northern Israel, notably those in Mount Carmel (e.g. Garrard, 1982; Weinstein-Evron et al., 2003; Yeshurun et al., 2007; Speth, 2012; Marín-Arroyo, 2013): Persian fallow deer (*Dama mesopotamica*), mountain gazelle (*Gazella gazella*), aurochs (*Bos primigenius*), ostrich (*Struthio camelus*) and spur-thighed tortoise (*Testudo graeca*).

Four species of Mediterranean marine shells were also recovered - *Donax trunculus, Cerastoderma traucum*, *Acanthocardia tuberculata* and *Glycymeris nummaria* (previously *G. insubrica*) (Ronen et al., 2008). A well rounded perforation in the umbo of one of the *G. nummaria* valves (Fig. 4d) may have been intentionally man-made. It has not been possible to establish whether the shells were introduced into the cave by hominins or a natural agent, especially since they were found close to the top of the cultural fill, albeit together with lithic artefacts and fauna. *Glycymeris* shells have been reported from MP layers in the inland sites of Skhul, Qafzeh and Sefunim (Bar-Yosef Mayer, 2005; Bar-Yosef Mayer et al., 2009), indicating that this marine mollusk was exploited by local hominins (in all instances, early *Homo sapiens*). At Skhul, aside from *G. nummaria*, other species of Mediterranean marine shells were also found; *Cardium* sp., *Nassarius gibbosulus* and *Pecten jacobaeus.* At these sites, the umbos' of the shells had natural perforations, but there was evidence of ochre staining and use-wear marks leading to the conclusion that they were used as ornaments (Bar-Yosef Mayer, 2005, Bar-Yosef Mayer et al., 2009). Moreover, it has been suggested that since the *G. nummaria* shells found in Sefunim Cave in Mount Carmel were abraded, that they were old shells intentionally collected for ornaments rather than for consumption (Bar-Yosef Mayer et al., 2009).

The small size of the recovered archaeological assemblage and the fact that it was collected rather than excavated, necessitates exercising some caution when interpreting these remains. However, it is possible that the ARB site and others like it functioned as sea-shore camps for collection of marine shells and other resources which were then taken or exchanged inland.

Luminescence dating

Samples for dating were collected from Cave II and Cave III infills, from deposits associated with bones and flint artifacts (Fig. 3). As the sediment is highly indurated, the samples were taken as blocks and were later cleaned and processed in a lab with appropriate low level orange lighting. Field and laboratory data are given in Table 2.

Quartz and feldspars were purified by gentle crushing of the blocks, sieving to the selected grain sizes, dissolving carbonates by 8% HCl, followed by a 2-step density separation at 2.62 gr/cm^3 and 2.58 gr/cm^3 using sodium-polytungstate. The quartz-rich fraction (heavier than 2.62 gr/cm^3) was further cleaned using magnetic separation (1.4 A on the Frantz magnetic separator) and etching with 40% HF (for 40 min), followed by soaking in 16% HCl to dissolve any fluorides which may have precipitated. The concentrated potassium feldspar (KF) grains (lighter than 2.58 gr/cm^3) were not etched.

Dose rates: Alpha, beta and gamma dose rates (Table 2) were calculated from the concentrations of the radioactive elements in the sediment measured by atomic absorption spectroscopy (K) or inductively coupled plasma mass-spectrometry (U and Th), with relative errors of 3%, 5% and 10%, respectively, and attenuation factors as in Nambi and Aitken (1986). Although the measured K-contents of the KF range from 10.5 to 11.1%, the internal beta dose rate for KF was calculated using a K-content of 12.0±0.5%. This value was selected as grains with the brightest infra-red stimulated luminescence (IRSL) signals have such K-contents (Smedley et al., 2012), and in multi-grain measurements such grains will dominate the signal. This value is somewhat lower than that suggested by Huntley and Beril (1997), 12.5±0.5%. The a-value was estimated at 0.15±0.05, an average of the values given for KF by Balescu et al. (2007) and Rendel et al. (1993). Cosmic dose rate was evaluated from burial depth of 8±1 m, at 85±8 μGy/a (Prescott and Hutton, 1994). Moisture contents were estimated at 10±3 %.

The measured signals: Four different luminescence signals were used to determine the equivalent dose (De) values, and five De values were obtained for each sample to be used in the age calculations. Measurements were carried out using Risø TL/OSL readers

equipped with calibrated ^{90}Sr beta sources either at the Geological Survey of Israel or at the DTU Nutech, Denmark. Measurement protocols are listed in Table 3.

Quartz optically stimulated luminescence (OSL) De was measured on 2-mm aliquots using blue LED stimulation with detection through 7.5 mm U-340 filters. Both the single aliquot regenerative dose (SAR; Table 3a; Murray and Wintle, 2000) and the single aliquot regenerated and added dose (SARA; Mejdahl and Bøtter-Jensen, 1994; Murray et al., 1995) protocols were used. The latter is used to check for any sensitivity change which may have occurred in the first measurement cycle and is not corrected for by the first test dose normalization (Table 3a). Twenty-four aliquots were used to construct the SARA plot, whereby the De is measured using the SAR protocol on several aliquots of the natural sample, as well as on aliquots of the natural sample that received a range of added laboratory doses. The measured De is plotted against the added doses and the intercept of the SARA curve with the added dose axis is the natural De (Fig. 6). A slope of unity indicates that no sensitivity change took place in the first measurement cycle

Quartz violet stimulated luminescence (VSL) was measured on 8-mm aliquots using the SAR protocol in Table 3b (modified from Jain 2009). Stimulation was with a solid state violet (405 nm) laser diode and a setup as in Jain (2009). Detection was through a 7.5mm U340 filter combined with a Semrock Brighline 340 nm interference filter (Ankjaegaard et al., 2013).

Alkali feldspar infrared stimulated luminescence (IRSL) was measured on 2-mm aliquots in stainless steel cups using the SAR protocol in Table 3c (Thiel et al. 2011) which measures both the IR_{50} and the $pIRIR_{290}$ signals. Stimulation was by IR diodes (880 nm) and detection was through a Schott BG-39 and a Corning 7-59 filter pack, used to cut off the IR stimulation and relatively enhance the violet emission from the KF. Anomalous fading was measured for the three samples (six aliquots each) for up to 44 hours following Buylaert et al. (2008) and the IR_{50} ages were corrected for the measured fading rates as in Huntley and Lamothe (2001) using the R luminescence package (2015).

For all samples and signals the average and errors were calculated using the central age model (CAM; Galbraith and Roberts, 2012). For SARA the error on the De was calculated from the goodness of fit.

Luminescence Results

Typical luminescence signals, dose response curves and De distribution (as probability density functions) are shown in Figure 7 for the OSL, $pIRIR_{290}$ and VSL signals. Figure 7 (panels c. f. and i.) and Table 2 show that the $pIRIR_{290}$ measurements are the least scattered, with overdispersion (OD) values of 6-8%. For two of the three samples, quartz OSL is less scattered than quartz VSL.

OSL: overall the OSL signal is dominated by the fast component (Fig. 7a). Quality assurance parameters show that the SAR protocol can correct for sensitivity changes (recycling ratios within 10% of unity), there is no IR contamination (IR depletion ratio >0.9), recuperation is negligible, and the natural OSL signal is far from saturation (D_0 = 45-55 Gy). SARA results are shown for sample ATL-1 (Fig. 6). The slope of the fitting line is 0.9, suggesting that most sensitivity changes taking place in the first SAR cycle are corrected for adequately by the first test dose. The De calculated from the intercept, 54.6 ± 6.6 Gy, agrees very well with the conventional SAR De, 51.5 ± 2.7 Gy (Table 2).

VSL: Fig. 7g shows a natural and regenerated VSL signals from sample ATL-4, and Figure 7h presents a VSL dose response curve. The signal is overall weak and the data points on the DRC are often scattered; these were fitted with a double saturating exponential. Poor recycling ratios and high recuperation are prevalent. A comparison of the DRCs for quartz OSL and VSL (Figs. 7b and 7h, respectively) shows that, while the curves cannot be compared directly due to different test doses, the DRCs from both signals have an onset of saturation at similarly low doses, and both signals have typical D_0 of 45-65 Gy. A range of preheats in the VSL SAR protocol was tested to explore the possibility of reducing recuperation and increasing the D_0 values. Increasing the preheat and cutheat temperatures to 310ºC and 300ºC, respectively, increased the VSL D_0 to about 100 Gy. It also decreased recuperation; however signal intensity decreased even further.

335

336 *IRSL*: The ratio between the De values calculated from the IR_{50} and $pIRIR_{290}$ signals is
337 0.5-0.6. Average measured fading rates were 2.9±0.5 and 0.4±0.3 % per decade for the
338 IR_{50} and $pIRIR_{290}$ signals, respectively, rendering fading corrections for the $pIRIR_{290}$
339 signal unnecessary. Even after correcting for fading, the IR_{50} ages are 20-25% lower
340 than the $pIRIR_{290}$ ages (Table 2). As the corrected IR_{50} ages are also younger than the
341 quartz VSL and OSL ages, it appears that the measured fading rates might not represent
342 fading in nature.
343

344 *The ages:* The ages obtained using the different minerals, luminescence signals and
345 measurement protocols are overall comparable (Fig. 8), and in most cases are within
346 errors of each other (notably, the VSL age for ATL-4 and the corrected IR_{50} age for
347 ATL-2 are younger than the other results). Evidently, the hard-to-bleach signals such as
348 the VSL and $pIRIR_{290}$ do not give higher ages, indicating that both quartz and feldspar
349 grains were well bleached at the time of deposition. Samples ATL-1 and ATL-2 are
350 from the same unit, and indeed their averaged ages are very similar, 87±9 ka and 91±9
351 ka, respectively. Although the De values for both minerals of sample ATL-4 are similar
352 to the other two samples (Table 2), the dose rate is higher, resulting in a younger
353 averaged age of 71±10 ka.
354

355 ## Discussion

356

357 The luminescence ages obtained here for the Atlit Railway Bridge sediments using four
358 different signals show good correspondence. They also agree with the general
359 chronostratigraphy presented by Frechen et al. (2004), but offer further refinement. We
360 can better understand the sequence of events leading to cave formation and infill if we
361 correct the IRSL ages in Frechen et al. (2004), measured at 50ºC, to fading rates
362 measured from adjacent samples in this study.
363

364 The IR_{50} De values presented here, that were measured for the ARB samples using the
365 $pIRIR_{290}$ SAR protocol (Table 3c), can be compared to De measurements carried out in
366 the past on the same samples using the IR_{50} signal and the single aliquot added dose
367 (SAAD) protocol (Duller, 1994), although preheats differed – 10 s at 290ºC and 600 s at

220ºC, respectively. The SAAD De values (and hence the ages) are 10-13% lower than the SAR values, perhaps due to the lower preheat used for the SAAD. Nonetheless, as the SAAD IR_{50} values are not far removed from the currently measured SAR IR_{50} values, our measured fading rates can be used to correct IRSL ages measured in the past. The corrected ages should be taken only as a rough estimate of depositional age, as measurement protocols differed and the fading measurements carried out in this study were devised to correct for the SAR protocol (Auclair et al., 2003).

If we take this approach and correct the ages presented in Figure 2 using the averaged g-value of 2.9±0.5 measured for the ARB samples, then the fading-corrected ages are as follows:

Unit 1 kurkar that hosts the caves (Fig. 2): 195±42 ka.

Unit 4 kurkar: 182±37 ka.

Unit 5 paleosol: 96±11 ka.

Units 6 kurkar: 76±19 ka.

Unit 7 soil: 15±3 ka.

The age of the beachrock filling the cave and underlying the archaeological beds is most likely ~125 ka (Galili et al., 2007). Thus, the lower kurkar units were deposited during MIS 7-6, the caves formed during the MIS 5e high sea-stand and soon after were partially filled with beachrock, and at ~90 ka and ~70 ka the caves were frequented by hominins, roughly at the same time when a soil formed at the top (Unit 5). The upper kurkar was deposited during MIS 4, at the same time interval that kurkar was deposited further to the south in the Sharon coast (Porat et al., 2004).

Taking all the ages obtained here, the best estimate of the time of deposition of the sediments embedding the lithic artifacts and fauna in Cave III is ~90 ka, and that of Cave II is ~70 ka. Possibly, the caves were used at different times as hominins were present in the region throughout these prehistoric periods.

The age range for Cave III, ~ 80-100 ka, is comparable to the ages of the Mousterian Layer B in Tabun (104+30/-18 ka; Grün and Stringer, 2000) and is only somewhat younger than the Levantine-Mousterian found in Skhul (100-130 ka; Grun et al., 2005), located only 6 km to the south-east (Fig. 1).

The range of Cave II, 71±10 ka, is comparable to that of the Mousterian site of Ein Qashish of 64±4 ka, located 15 km inland as the crow flies (Greenbaum et al. 2014). Other late MP sites occur in the vicinity of Mount Carmel, but this is the only open air site to have been dated so far. While the direct aerial route between Atlit and Ein Qashish might be challenging - given that one would have to traverse Mount Carmel – other more amenable routes to the coast, via either the Qishon Valley or Wadi Mileq, are only ~35 km long. The relative proximity of these sites suggests that sorties to the coast by inhabitants located further inland such as Ein Qashish, may have taken place. This option is highlighted by the presence of Mediterranean seashells in the MP site of Qafzeh, located ~45 km inland from the coast (Bar-Yosef Mayer et al., 2009).

Two MP hominin populations inhabited Mount Carmel close to the Atlit caves - Neanderthals and modern humans (Garrod and Bate, 1937; McCown and Keith, 1939; Shea, 2010), over a period estimated by uranium series/ESR and TL dating to 165-100 ka (Mercier and Valladas, 2003; Grün et al., 2005). We can envisage a scenario whereby the hominins (Neanderthals and/or modern *Homo*) living in the Carmel caves and other inland sites visited the coast and occupied the smaller caves and other open air localities found within the coastal aeolianites (Ronen and Chernikov, 2010). Even with lowered sea level in MIS 5a of up to -30 m, the coastline was only 3-5 km away from Atlit. Given the ephemeral nature of occupation at ARB (shallow deposits, few finds, lack of evidence for on-site knapping), these late MP coastal occupations appear to represent short-lived camp sites, perhaps specifically focused on exploitation of marine and other coastal resources, rather than long term occupations such as known from the coeval Levantine caves (see discussion in Zaidner et al., 2016).

To place ARB within the larger chronological framework of the Middle Paleolithic of the southern Levant, we compared the ARB aged to those compiled for MP sites in the southern Levant by Shea (2010; 2013). Shea (2013) divides the time frame of the MP into three main groupings: Phase 1, Early Mousterian that ranges from 240 to 130 ka, encompassing MIS 7 and 6; Phase 2, Middle Mousterian ranging from 130 to 75 which overlaps MIS 5; and Phase 3, Later Mousterian that starts at roughly 75 ka and ends with the MP at ~49 ka (Rebollo et al., 2011), marking the transition to the Upper Paleolithic. From this division it is evident that the ARB ages fall in the transition between Phases 2 and 3. The lithic typology of the small assemblage of flakes and

artefacts recovered from the ARB site show affinities to Tabun Layer C and B type industries, which according to Culley et al. (2013) demonstrate a high statistical affinity to each other. The age of ARB site thus suggests that hominins exploited Mediterranean coastal environments in the southern Levant, at least since 90 ka.

Conclusions

The two caves containing archaeological remains at Atlit Railway Bridge were dated by luminescence methods using four different signals, OSL, VSL, (fading corrected) IR_{50} and $pIRIR_{290}$. The resulting ages show great consistency which increases our confidence in the dating methods and the resulting ages. These place the occupation time of Caves III and II at ~90 and ~70 ka, respectively. After correcting the ages presented by Frechen et al. (2004) for anomalous fading, the kurkar in which the caves formed can be attributed to MIS 7 and 6, the cave infill within MIS 5 and the top of the kurkar section to MIS 4.

When placed within the cultural-chronological scheme published by Shea (2013), the occupation at ARB falls around the transition from middle to late MP in the region. This unique occurrence of lithics and fauna represents a coastal camp site occupied by hominins during the second half of the Mousterian, and is probably related to increased foraging mobility during MIS 5. The ARB site, though represented by a small collection of finds, expands our understanding of the repertoire of behaviors and sites occupied during the Levantine late MP.

Acknowledgements:
NP thanks DTU Nutech for facilitating her visit there in 2013 and the VSL measurements. We thank S. Zeffren for sample preparation and the Geochemistry laboratories at the GSI for chemical analyses of the sediments.

References

Akazawa, T., Aoki, K. and Bar-Yosef, O. (eds). 1998. *Neandertals and Modern Humans in Western Asia*, New York & London: Plenum Press.

Almagor, G. 2002. *The Mediterranean Coast of Israel*. Jerusalem: Geological Survey of Israel.

Ankjærgaard, C., Jain, M. and Wallinga, J. 2013. Towards dating quaternary sediments using the quartz violet stimulated luminescence (VSL) signal. *Quaternary Geochronology* 18, 99-109.

Auclair, M., Lamothe, M., Huot, S., 2003. Measurement of anomalous fading for feldspar IRSL using SAR. *Radiation Measurements* 37, 487-492.

Balescu, S., Ritz, J.-F., Lamothe, M., Auclair, M. and Todbileg, M. 2007. Luminescence dating of a gigantic palaeolandslide in the Gobi-Altay mountains, Mongolia. *Quaternary Geochronology* 2, 290-295.

Bar-Yosef O. 2002. The Upper Paleolithic revolution. *Annual Review of Anthropology*, 31, 363-393.

Bar-Yosef, O., & Meignen, L. 1992. Insights into Levantine Middle Paleolithic cultural variability. In H. L. Dibble & P. Mellars (Eds.), *The Middle Paleolithic: Adaptation, Behavior, and Variability* (pp. 163–182). University Museum Monograph 78. University Museum, University of Pennsylvania, Philadelphia.

Bar-Yosef, O. and Pilbeam, D. (eds.) 2000. *The Geography of Neandertals and Modern Humans in Europe and the Greater Mediterranean*. Peabody Museum, Harvard University, Cambridge, Massachusetts.

Bar-Yosef, O. and Meignen, L. (eds.). 2007. *Kebara Cave Mt. Carmel, Israel. The Middle and Upper Paleolithic Archaeology. Part I*. Harvard University, Cambridge, American School of Prehistoric Research Bulletin 49. Peabody Museum of Archaeology and Ethnology.

Bar-Yosef Mayer, D.E., 2005. The exploitation of shells as beads in the Palaeolithic and Neolithic of the Levant. *Paléorient* 31/1, 176-185.

Bar-Yosef Mayer, D.E., Vandermeersch, B. and Bar-Yosef, O. 2009. Shells and ochre in Middle Paleolithic Qafzeh Cave, Israel: Indications for modern behavior. *Journal of Human Evolution* 56, 307-314.

Belfer-Cohen, A. and Goring-Morris, A.N. 2009. The shift from the Middle Palaeolithic to the Upper Palaeolithic: Levantine perspectives. In: M., Camps, and C. Szmidt (Eds.), *The Mediterranean from 50,000 to 25,000 BP: Turning Points and New Directions* (pp.89-100). Oxbow Books, Oxford.

501 Belfer-Cohen, A. and Hovers, E. 2010. Modernity, enhanced working memory, and the
502 Middle to Upper Paleolithic record in the Levant. *Current Anthropology*, 51 (S1),
503 S167-S175.
504 Bronk Ramsey, C. 2009. Bayesian analysis of radiocarbon dates. *Radiocarbon* 51, 337-
505 360.
506 Bronk Ramsey, C., Higham, T.F G., Bowles, A., and Hedges, R. 2004. Improvements to
507 the pretreatment of bone at Oxford. *Radiocarbon* 46, 155-163.
508 Buylaert, J.P., Murray, A.S. and Huot, S. 2008. Optical dating of an Eemian site in
509 Northern Russia using K-feldspar. *Radiation Measurements* 43, 715-720.
510 Buylaert, J.-P., Murray, A.S., Thomsen, K.J. and Jain, M. 2009. Testing the potential of
511 an elevated temperature IRSL signal from K-feldspar. *Radiation Measurements*
512 44, 560–565.
513 Culley E.V., Popescu G. and Clark G.A. 2013. An analysis of the compositional
514 integrity of the Levantine Mousterian facies. *Quaternary International* 300, 213-
515 233.
516 Duller, G.A.T., 1994. Luminescence dating of sediments using single aliquots: new
517 procedures. *Quaternary Geochronology* (*Quaternary Science Review*) 13, 149-
518 156.
519 Eytam, Y. and Ben-Avraham, Z. 1992. Morphology and sediments of the inner shelf off
520 northern Israel. *Israel Journal of Earth Science* 41, 27-44.
521 Frechen, M., Neber, A., Dermann, B., Tsatskin, S., Boenigk, W. and Ronen, A. 2002.
522 Chronostratigraphy of aeolianites from the Sharon coastal plain of Israel.
523 *Quaternary International* 89, 31-44.
524 Frechen, M., Neber, A., Tsatskin, A., Boenigk, W. and Ronen, A. 2004. Chronology of
525 Pleistocene sedimentary cycles in the Carmel coastal plain of Israel. *Quaternary*
526 *International* 121:1–52.
527 Galbraith, R.F. and Roberts, R.G. 2012. Statistical aspects of equivalent dose and error
528 calculation and display in OSL dating: an overview and some recommendations.
529 *Quaternary Geochronology* 11, 1-27.
530 Galili, E., Zviely, D., Rosen, B. and Mienis, H. K. 2007. Beach deposits of MIS 5e high
531 sea stand as indicators for tectonic stability of the Carmel coastal plain, Israel.
532 *Quaternary Science Reviews* 26, 2544-2557.

533 Galili, E., Ronen, A., Mienis, H.K, Horwitz, L.K. (this volume). Beach deposits
534 containing Middle Paleolithic archaeological remains from northern Israel.
535 *Quaternary International* (in press).
536 Garrard, A.N. 1982. The environmental implications of a reanalysis of the large
537 mammal fauna from Wadi El-Mughara caves, Palestine. In: J. L. Bintliff and W.
538 Van Zeist (Eds.), Palaeoclimates, Palaeoenvironments and Human Communities
539 in the Eastern Mediterranean Region in Later Prehistory. Oxford, BAR
540 International Series 133, pp. 165-187.
541 Garrod, D.A.E. and Bate D.M.A. 1937. *The Stone Age of Mount Carmel: Excavations at*
542 *the Wady el-Mughara, Vol. I.* Oxford: Clarendon Press.
543 Gignoux, M., 1913. Les formations marines Pliocénes et quaternaries de l`Italie de sud
544 et la Sicilie. Annales de l`Universite de Lyon, 36.
545 Goren-Inbar N. and Belfer-Cohen A. 1998. The technological abilities of the Levantine
546 Mousterians: cultural and mental capacities. In: T. Akazawa, K .Aoki and O. Bar-
547 Yosef (Eds.), *Neandertals and Modern Humans in Western Asia*, pp. 205-222.
548 New York: Plenum Press.
549 Greenbaum, N., Ekshtian, R., Malinsky-Buller, A., Porat, N. and Hovers E. 2014. The
550 stratigraphy and paleogeography of the Middle Paleolithic open-air site of 'Ein
551 Qashish, northern Israel. *Quaternary Science Reviews* 103, 153-169.
552 Grün, R. 2006. Direct dating of human fossils. *Yearbook of Physical Anthropology* 49,
553 2-48.
554 Grün, R. and Stringer, C.B. 2000. Tabun revisited: revised ESR chronology and new
555 ESR and U-series analyses of dental material from Tabun C1. *Journal of Human*
556 *Evolution* 39, 601-612.
557 Grün, R., Stringer, C., McDermott, F., Nathan, R., Porat, N., Robertson, S., Taylor, L.,
558 Mortimer, G., Eggins, S. and McCulloch, M. 2005. U-series and ESR analyses of
559 bones and teeth relating to the human burials from Skhul. *Journal of Human*
560 *Evolution* 49, 316-334.
561 Henry, D.O. 1992. The impact of radiocarbon dating on Near Eastern prehistory. In: R.
562 E. Taylor, A. Long, R.S. Kra (Eds.), *Radiocarbon after Four Decades*. Springer
563 Science & Business Media, New York. Pp. 324-334.
564 Hershkovitz I., Marder, O., Ayalon, A., Bar-Matthews, M., Yasur, G., Boaretto, E. and
565 18 others, 2015. Levantine cranium from Manot Cave (Israel) foreshadows the
566 first European modern humans. *Nature* 520, 216-219.

567 Hovers E. 2009. *The Lithic Assemblages of Qafzeh Cave*. Oxford University Press,
568 Oxford.
569 Huntley, D.J. and Baril, M.R. 1997. The K content of the K-feldspars being measured in
570 optical dating or in the thermoluminescence dating. *Ancient TL* 15, 11–13.
571 Huntley, D.J. and Lamothe, M. 2001. Ubiquity of anomalous fading in K-feldspars and
572 the measurement and correction for it in optical dating. *Canadian Journal of*
573 *Earth Science* 38,1093-1106.
574 Issar, A. 1968. Geology of central coastal plain of Israel. *Israel Journal of Earth*
575 *Science* 17, 16-29.
576 Jain, M. 2009. Extending the dose range: probing deep traps in quartz with 3.06 eV
577 photons. *Radiation Measurements* 44, 445-452.
578 Jelinek A.J. 1981. The Middle Paleolithic in the southern Levant from the perspective of
579 the Tabun Cave. In: J. Cauvin and P. Sanlaville (Eds.), *Préhistoire du Levant*.
580 Centre National de la Recherche Scientifique, Paris, pp 265–280.
581 Jelinek, A.J. 1982. The Middle Paleolithic in the Southern Levant, with comments on
582 the appearance of modern *Homo sapiens*. In: A. Ronen (Ed.), *The Transition from*
583 *Lower to Middle Paleolithic and the Origin of Modern Man*. Oxford, BAR
584 International Series 151, pp. 57-101.
585 Kadowaki, S. 2013. Issues of chronological and geographical distributions of Middle
586 and Upper Palaeolithic cultural variability in the Levant and implications for the
587 learning behavior of Neanderthals and *Homo sapiens.* In: T. Akazawa, Y.
588 Nishiaki, and K. Aoki (Eds.), *Dynamics of Learning in Neanderthals and Modern*
589 *Humans Volume 1: Cultural Perspectives*, Replacement of Neanderthals by
590 Modern Humans Series, Springer Japan, pp. 59-91.
591 Langdon, J. H. 2016. Case study 20. The Neanderthal problem: Neighbors and relatives
592 on Mt. Carmel. In: J.H**.** Langdon (Ed.), *The Science of Human Evolution.* Springer
593 International Publishing. pp. 159-166.
594 Marín-Arroyo, A.B. 2013. Paleolithic human subsistence in Mount Carmel (Israel). A
595 taphonomic assessment of Middle and Early Upper Paleolithic faunal remains from
596 Tabun, Skhul and el-Wad. *International Journal of Osteoarchaeology* 23, 254–273.
597
598 McCown, T.D. and Keith, A. 1939. *The Stone Age of Mount Carmel: The Fossil Human*
599 *Remains from the Levalloiso-Mousterian.* Vol. 2. Oxford: Clarendon Press.

600 Meignen, L., Bar-Yosef, O., Speth, J. D., Stiner, M. C., 2006. Middle Paleolithic
601 settlement patterns in the Levant. In: E. Hovers and S.L. Kuhn (Eds.), *Transitions*
602 *Before the Transition.* Springer US, pp.149-169.
603 Mejdahl, V. and Bøtter-Jensen, L. 1994. Luminescence dating of archaeological
604 materials using a new technique based on single aliquot measurements.
605 *Quaternary Geochronology (Quaternary Science Reviews)* 13, 551-554.
606 Mercier, N., Valladas, H., Falguères, C., Shao, Q., Gopher, A., Barkai, R., Bahain, J-J.,
607 Vialettes, L., Joron, J-L. and Reyss, J-L. 2013. New datings of Amudian layers at
608 Qesem Cave (Israel): Results of TL applied to burnt flints and ESR/U-series to
609 teeth. *Journal of Archaeological Science* 40, 3011-3020.
610 Murray, A.S., Olley, J.M. and Caitcheon, G.C. 1995. Measurement of equivalent doses
611 in quartz from contemporary water-lain sediments using optically stimulated
612 Luminescence. *Quaternary Geochronology* 14, 365-371.
613 Murray, A.S. and Wintle, A.G. 2000. Luminescence dating of quartz using an improved
614 single aliquot regenerative-dose protocol. *Radiation Measurements* 32, 57-73.
615 Nadel, D., Shtober, N., Frumkin, A. and Yaroshevich, A. 2012. New prehistoric cave
616 sites in lower Nahal Oren, Mt. Carmel, Israel. *Journal of the Israel Prehistoric*
617 *Society* 42, 75-114.
618 Nambi, K.S.V. and Aitken, M.J. 1986. Annual dose conversion factors for TL and ESR
619 dating. *Archaeometry* 28, 202-205.
620 Neber, A. 2002. Sedimentological properties of Quaternary Deposits on the Central
621 coastal plain. Unpublished Ph.D. dissertation. Dept. of Archaeology, University of
622 Haifa.
623 Olami, Y. 1984. *Prehistoric Carmel.* Jerusalem: Israel Exploration Society and the M.
624 Stekelis Museum in Haifa.
625 Orni, E. and Efrat, E.1971. *Geography of Israel*. Jerusalem: Israel Universities Press.
626 Porat, N., Wintle, A.G. and Ritte, M. 2004. Mode and timing of kurkar and hamra
627 formation, central coastal plain, Israel. *Israel Journal of Earth Sciences* 53, 13-25.
628 Prescott, J.R. and Hutton, J.T. 1994. Cosmic ray contribution to dose rates for
629 luminescence and ESR dating: Large depths and long-term time variations.
630 *Radiation Measurements* 23, 497-500.
631 R Luminescence Developer Team, 2015. Luminescence: Comprehensive Luminescence
632 Dating Data Analysis. *R package version 0.4.5.* URL: http://CRAN.R-
633 project.org/package=Luminescence.

Rak, Y. 1998. Does any Mousterian cave present evidence of two hominid species? In: T. Akazawa, K. Aoki. and O. Bar-Yosef (Eds.), *Neanderthals and Modern Humans in Western Asia*. Plenum, New York, pp. 353–366.

Rebollo, N. R., Weiner, S., Brock, F., Meignen, L., Goldberg, P., Belfer-Cohen, A., Bar-Yosef, O. and Boaretto, E.2011 New radiocarbon dating of the transition from the Middle to the Upper Paleolithic in Kebara Cave, Israel. *Journal of Archaeological Science* 38:2424-2433.

Rendell, H., Yair, A. and Tsoar, H. 1993. Thermoluminescence dating of period of sand movement and linear dune formation in the northern Negev, Israel. In: K. Pye (Ed.), The Dynamics and Environmental Context of Aeolian Sedimentary Systems, vol. 72. *Geological Society Special Publication*, pp. 69–74.

Roberts, R.G., Jacobs, Z., Li, B., Jankowski, N.R., Cunningham, A.C. and Rosenfeld, A.B. 2015. Optical dating in archaeology: thirty years in retrospect and grand challenges for the future. *Journal of Archaeological Science* 56, 41-60.

Ronen, A., 1977. Mousterian sites in red loam in the Carmel coastal plain. *Eretz Israel 13 (Stekelis volume)*. Israel Exploration Society, Jerusalem. Pp. 183–190.

Ronen, A. 1984. *Sefunim Prehistoric Site, Mount Carmel, Israel.* Oxford: BAR International Series 230.

Ronen, A., Tsatskin, A. and Laukhin, S.A., 1999. The genesis and age of Mousterian paleosols in the Carmel coastal plain, Israel. In: W. Davies, and R. Charles, (Eds.), *Studies in Honour of D.A.E. Garrod*. Oxbow Books, Oxford. pp. 135–151.

Ronen, A., Neber, A., Mienis, H., Horwitz, L.K., Frumkin, A., Boenigk, W. and Galili, E. 2008. A Mousterian occupation on an OIS 5e shore near the Mount Carmel Caves, Israel. In: Z. Sulgostowska and A.J. Tomaszewski (Eds.), *Man, Millennia, Environment. Studies in Honour of Romuald Schild*. Warsaw: Institute of Archaeology and Ethnology, Polish Academy of Sciences. pp 197-205.

Ronen, A. and Chernikov, I. 2010. The Mousterian of the red loam on the Carmel coast (Israel). In: J.M. Burdukiewicz, and A. Wisniewski (Eds.), *Middle Palaeolithic Human Activity and Palaeoecology: New Discoveries and Ideas.* Wroclaw University Press, Wroclaw, Pp. 425-446.

Shea, J. J. 2008. Transitions or turnovers? Climatically-forced extinctions of *Homo sapiens* and Neanderthals in the East Mediterranean Levant. *Quaternary Science Reviews* 27 (23-24): 2253–2270.

667 Shea, J.J., 2010. Neanderthals and early *Homo sapiens* in the Levant. In: E.A.A. Garcea
668 (Ed.), *South-Eastern Mediterranean Peoples between 130,000 and 10,000 years*
669 *Ago*. Oxford, Oxbow, pp. 126-143.
670 Shea, J.J., 2013. *Stone Tools in the Paleolithic and Neolithic Near East: A Guide.*
671 Cambridge University Press.
672 Sivan, D. and Porat, N. 2004. Evidence from luminescence for Late Pleistocene
673 formation of calcareous aeolianite (kurkar) and paleosol (hamra) in the Carmel
674 Coast, Israel. *Palaeogeography, Palaeoecology, Palaeoclimatology* 211, 95-106.
675 Smedley, R.K., Duller, G.A.T., Pearce, N.J.G., Roberts, H.M., 2012. Determining the K
676 content of single-grains of feldspar for luminescence dating. *Radiation*
677 *Measurements* 47, 790-796.
678 Speth, J.D. 2012. Middle Palaeolithic subsistence in the Near East: Zooarchaeological
679 perspectives – past, present and future. *Before Farming* 2: 1-45.
680 Thiel, C., Buylaert, J-P, Murray, A., Terhorst, B., Hofer, I., Tsukamoto, S. and Frechen,
681 M. 2011. Luminescence dating of the Stratzing loess profile (Austria) - testing
682 the potential of an elevated temperature post-IR IRSL protocol. *Quaternary*
683 *International* 234, 23-31.
684 Tsatskin, A. and Ronen, A. 1999. Micromorphology of a Mousterian paleosol in
685 aeolianites at the site Habonim, Israel. *Catena* 34, 365-384.
686 Valladas, H., Mercier, N., Hershkovitz, I., Zaidner, Y., Tsatskin, A., Yeshurun, R.,
687 Vialettes, L., Joron J-L., Reyss, J-L. and Weinstein-Evron, M. 2013. Dating the
688 Lower to Middle Paleolithic transition in the Levant: A view from Misliya Cave,
689 Mount Carmel, Israel. *Journal of Human Evolution* 65, 585-593
690 Weinstein-Evron, M., Bar-Oz, G., Zaidner, Y., Tsatskin, A., Druck, D., Porat, N. and
691 Hershkovitz, I. 2003. Introducing Misilya Cave, Mount Carmel, Israel: A new
692 continuous Lower/Middle Paleolithic sequence in the Levant. *Eurasian Prehistory*
693 1,31-55.
694 Weinstein-Evron, M. 2015. The case of Mount Carmel: The Levant and human
695 evolution, future research in the framework of World Heritage. In: N. Sanz (Ed.),
696 *Human Origin Sites and the World Heritage Convention in Eurasia Vol. 1*.
697 HEADS 4. Paris: UNESCO. Pp. 72-92. (http://creativecommons.org/licenses/by-
698 sa/3.0/igo/).
699 Weinstein, J.M. 1984. Radiocarbon dating in the southern Levant. *Radiocarbon 26,*
700 297-366.

Wintle, A.G. 2008. Luminescence dating: where it has been and where it is going. *Boreas* 37, 471-482.

Yeshurun, R., Bar-Oz, G., and Weinstein-Evron, M. 2007. Modern hunting behavior in the early Middle Paleolithic: Faunal remains from Misliya Cave, Mount Carmel, Israel. *Journal of Human Evolution* 53, 656-677.

Zaidner, Y., Frumkin, A., Friesem, D., Tsatskin, A., Shahack-Gross, R., 2016. Landscapes, depositional environments and human occupation at Middle Paleolithic open-air sites in the southern Levant, with new insights from Nesher Ramla, Israel. *Quaternary Science Reviews* 138, 76-86.

Figure captions:

Figure 1: Location map showing the Atlit Railway Bridge site (open circle marked with A) and the Sefunim (F), Tabun (T), Skhul (S), Misliya (M) and Kebara (K) caves nearby (modified from Frechen et al., 2002).

Figure 2: A log of the outcrop of aeolianites at the crossing of Highway 2 and the Atlit Railway Bridge. Three caves (marked with circled numbers 4, 9 and 10) are filled with beachrock and aeolianites that contain hearths, artifacts and faunal remains (section modified from Neber, 2002). Cave 9 (Cave III on Fig. 3 and in text) and Cave 10 (Cave II on Fig. 3 and in text) were sampled for this study. The sediments above and below the southern-most cave were previously dated by Frechen et al. (2004) using IRSL and the multiple aliquot added dose protocol (ages in ka marked within white rectangles).

Figure 3: The caves at Atlit Railway Bridge site with sampling locations. a. Cave III, now full of collapsed debris. Samples were collected from the underlying cave infilling sediments. b. Close-up of samples in Cave III. Yellow arrow shows the same rock in the two images. c. Cave II showing the different sedimentary units, the location of artifacts, fauna and OSL sample (modified from Ronen et al., 2008).

Figure 4: Faunal remains from Cave II: A. (clockwise from left: Tortoise (*Testudo graeca*) left hypoplastron, Fallow deer (*Dama mesopotamica*) left scapula neck; fragment of medium-mammal tibia shaft). B. Mountain gazelle (*Gazella gazella*) left proximal tibia. C. Gazelle right tibia distal epiphysis. D. *Glycymeris nummaria* marine shells showing holes in umbos' which may be man-made.

Figure 5: Atlit Railway Bridge lithics from Cave II (clockwise): A. Simple straight side scraper; B. Levallois flake – the piece has white patina except for the facets marked with a 'b' which are unpatinated brown flint; C. Backed knife; D. Levallois 'debordant' flake; E. Photograph of Levallois flake embedded in the kurkar.

Figure 6: A plot of the added dose against measured De (SARA) for OSL, sample ATL-4. The fit on the line through the data points is shown.

Figure 7: Luminescence signals (top), dose response curves (center) and probability density function (bottom) for each of the measured minerals and signals: Left – OSL on quartz; middle – $pIRIR_{290}$ on potassium feldspars; right – VSL (violet stimulated luminescence) on quartz.

Figure 8: A summary of all the ages obtained using the different luminescence signals and protocols for the Atlit Railway Bridge samples. The average age for each sample is shown by a large, full orange circle.

Table captions:

Table 1: Fauna identified from the Atlit Railway Bridge site.

Table 2: Luminescence dating field and laboratory data, dose rates and ages.

Table 3: Luminescence dating measurement protocols.

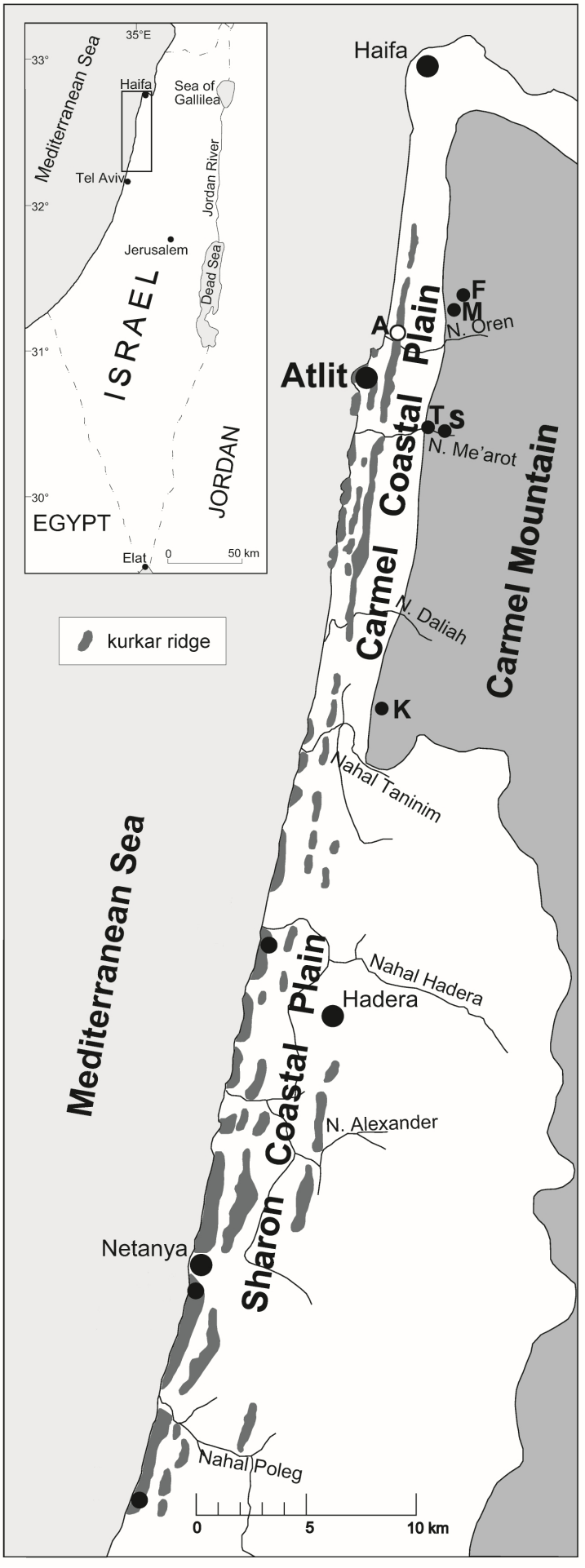
35°E
33°
32°
31°
30°
Mediterranean Sea
Haifa
Sea of Gallilea
Jordan River
Tel Aviv
Jerusalem
Dead Sea
ISRAEL
JORDAN
EGYPT
Elat
0
50 km
kurkar ridge
Haifa
F
M
N. Oren
A
Atlit
Ts
N. Me'arot
Carmel Coastal Plain
Carmel Mountain
N. Daliah
K
Nahal Taninim
Mediterranean Sea
Nahal Hadera
Hadera
Sharon Coastal Plain
N. Alexander
Netanya
Nahal Poleg
0
5
10 km

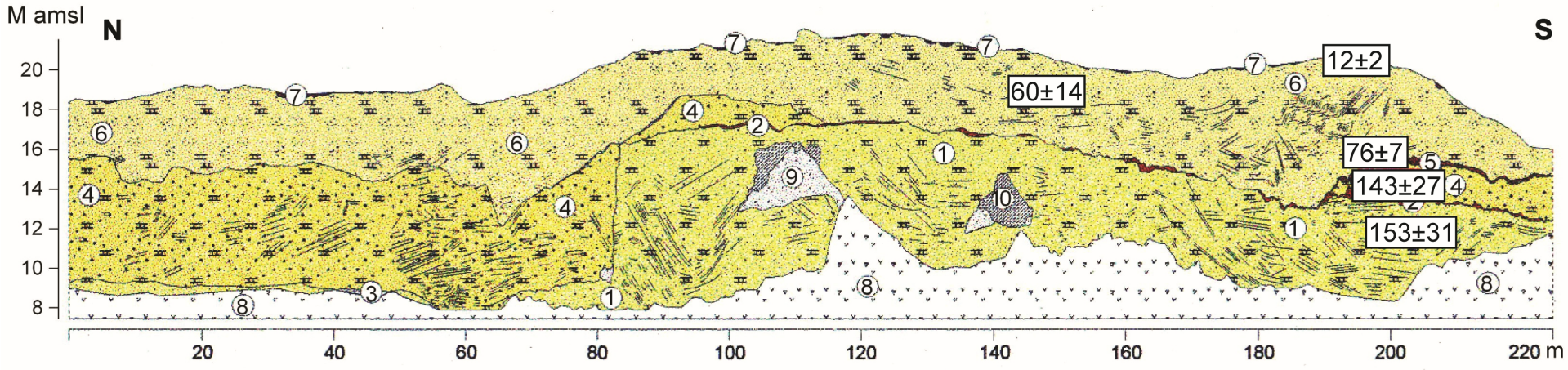

① lower aeolianite
② lower loam
③ beachrock
④ middle aeolianite
⑤ middle loam
⑥ upper aeolianite
⑦ upper loam
⑧ modern debris
⑨ cave II
⑩ cave III
Ky luminescence age estimate


a.
Cave III


b.
ATL-2
ATL-1
Cave III

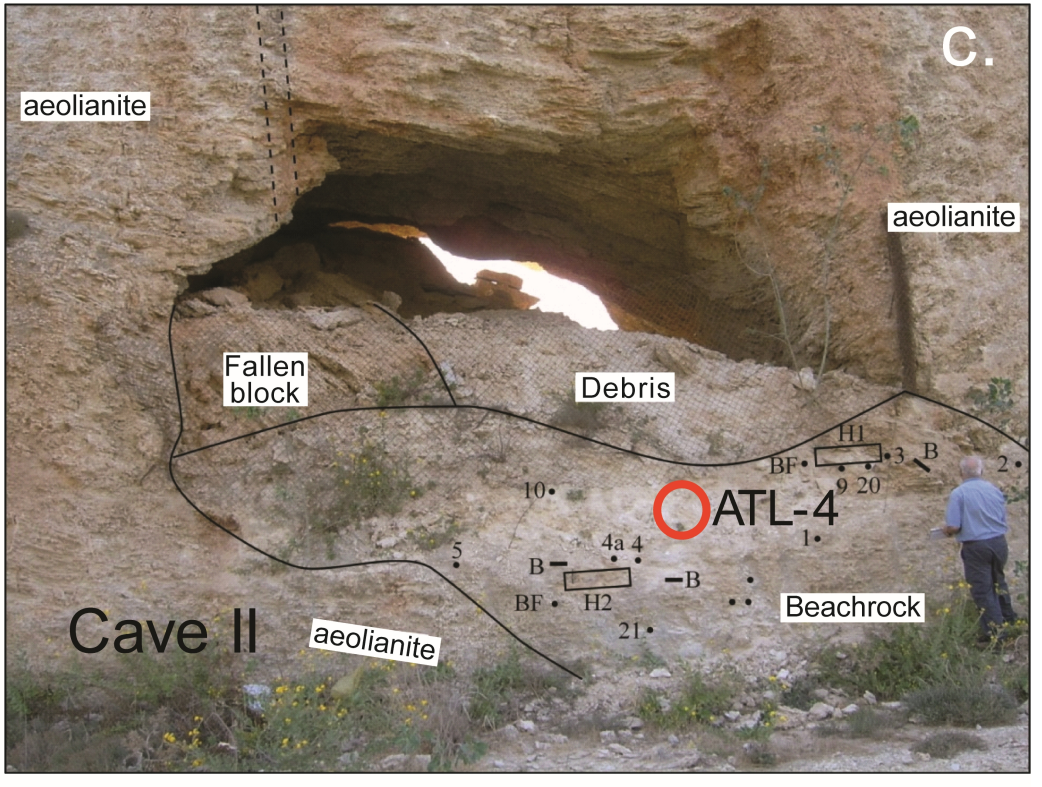
c.
aeolianite
aeolianite
Fallen block
Debris
H1
BF
3
B
2
9 20
10
ATL-4
1
5
4a 4
B
B
BF
H2
21
Beachrock
Cave II
aeolianite


A


B

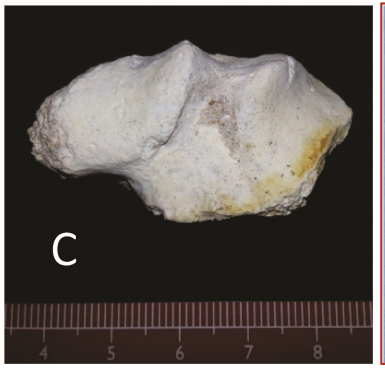
C


D

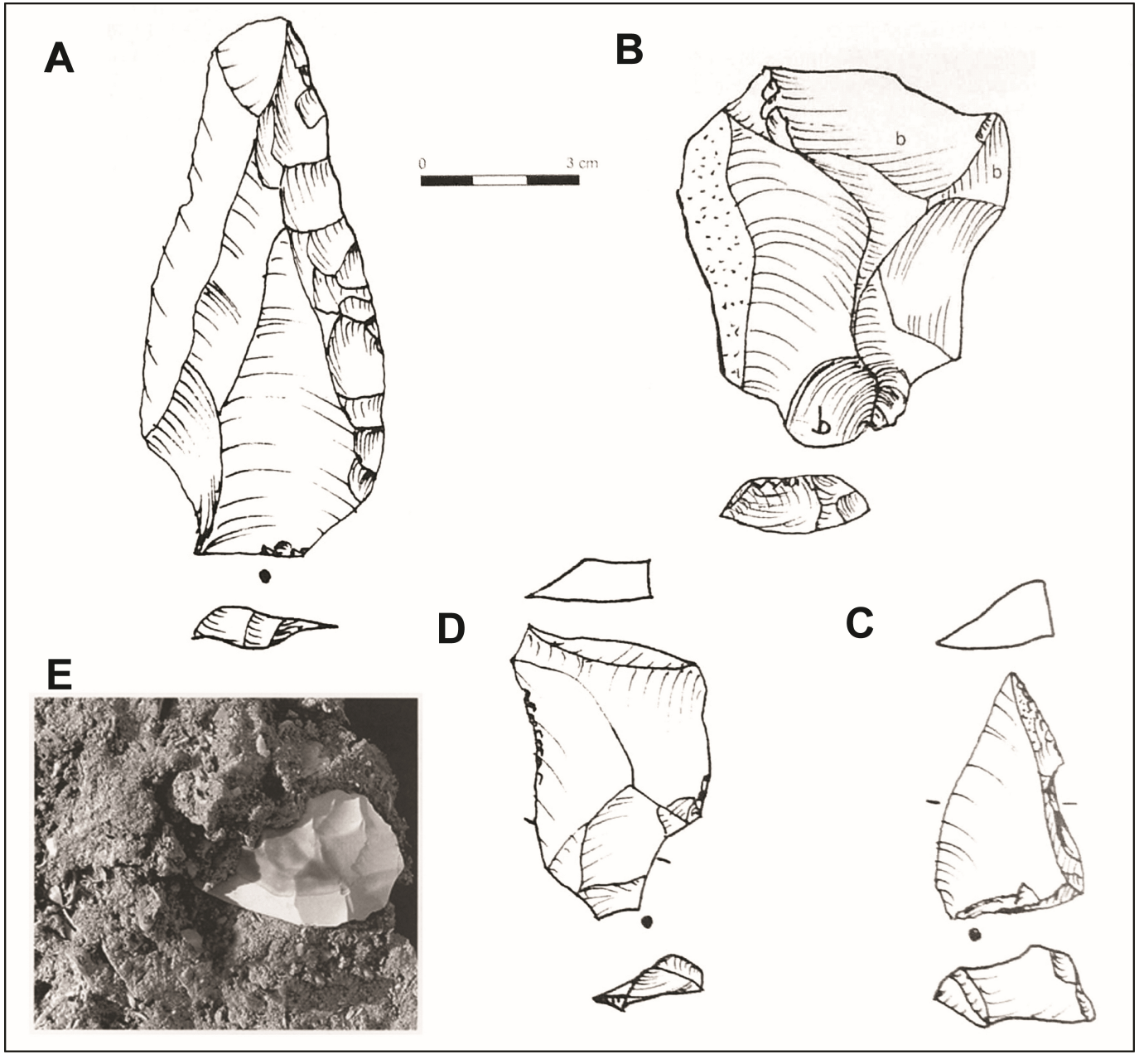
A
B
0
3 cm
b
b
b
D
C
E

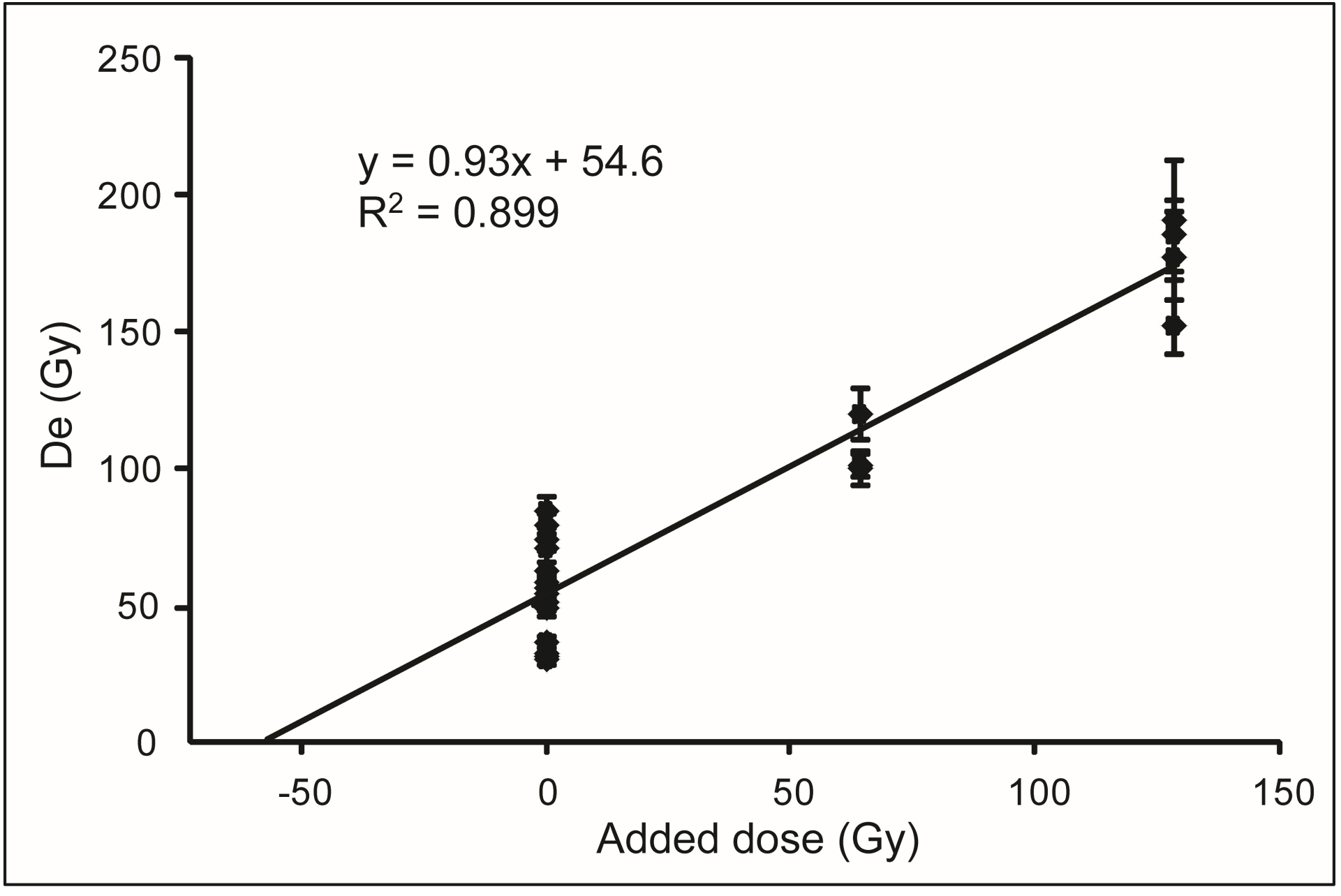
y = 0.93x + 54.6
R2 = 0.899
De (Gy)
Added dose (Gy)
250
200
150
100
50
0
-50
0
50
100
150

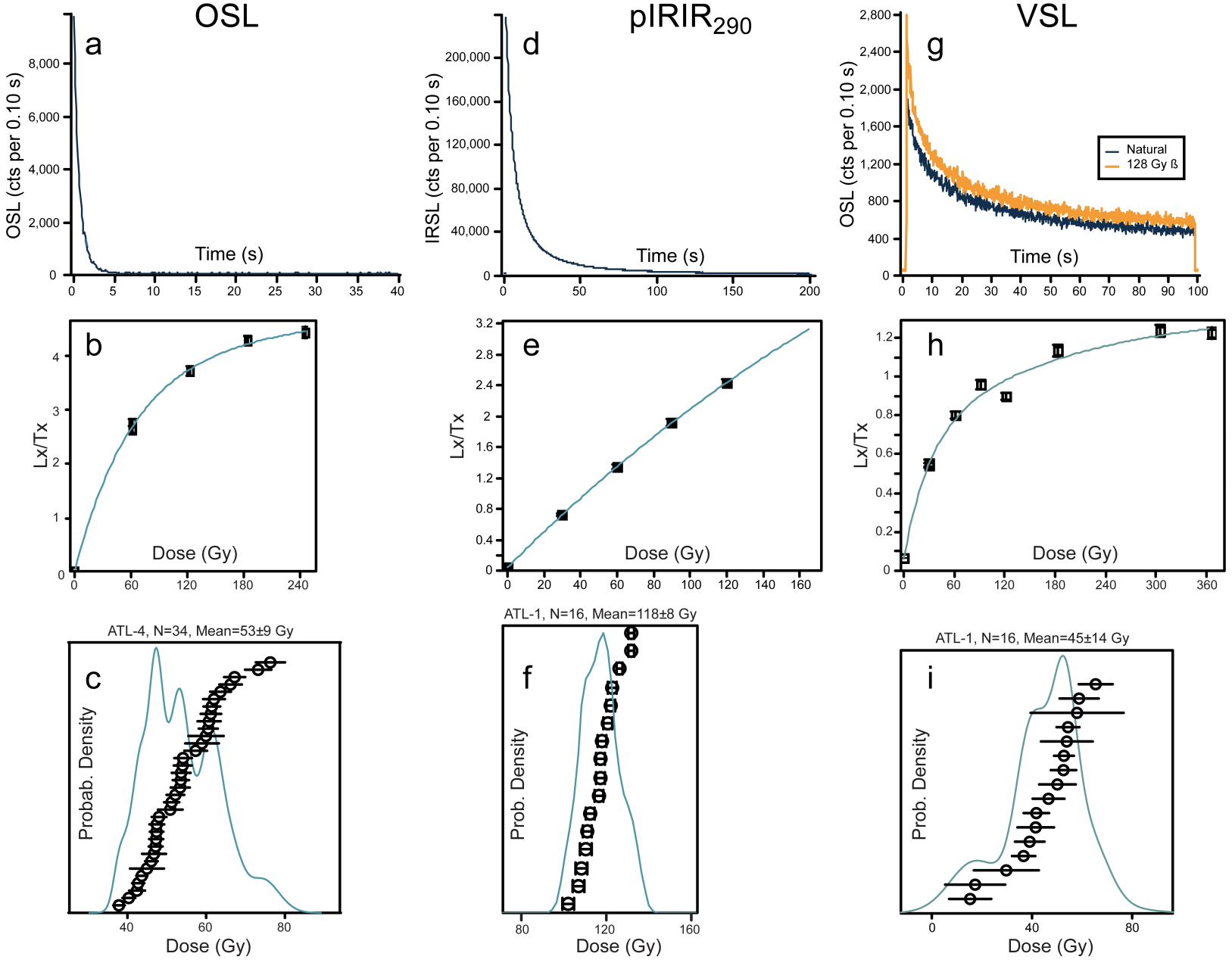
OSL
a
OSL (cts per 0.10 s)
Time (s)
b
Lx/Tx
Dose (Gy)
ATL-4, N=34, Mean=53±9 Gy
c
Probab. Density
Dose (Gy)
pIRIR290
d
IRSL (cts per 0.10 s)
Time (s)
e
Lx/Tx
Dose (Gy)
ATL-1, N=16, Mean=118±8 Gy
f
Prob. Density
Dose (Gy)
VSL
g
OSL (cts per 0.10 s)
Natural
128 Gy ß
Time (s)
h
Lx/Tx
Dose (Gy)
ATL-1, N=16, Mean=45±14 Gy
i
Prob. Density
Dose (Gy)

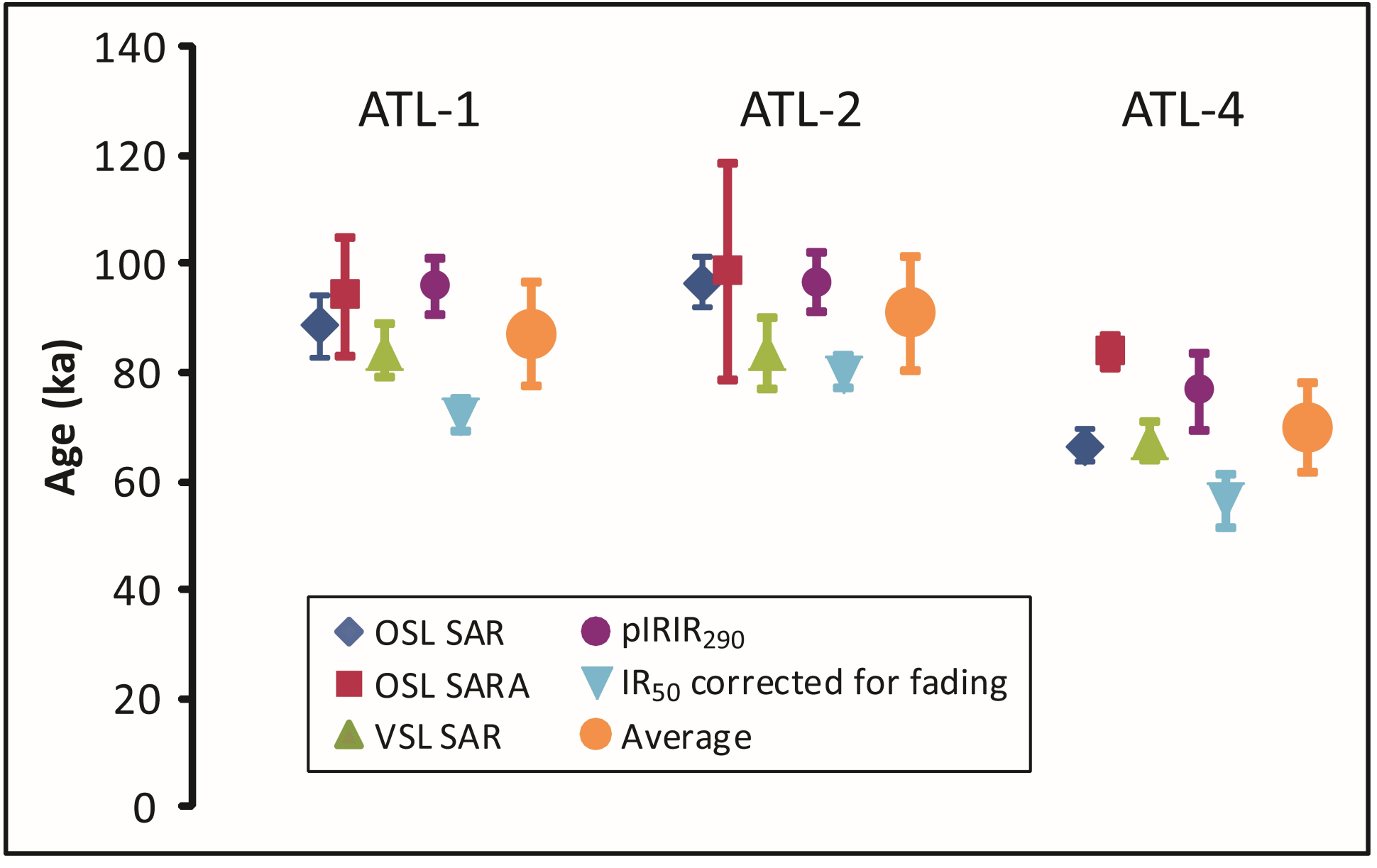
140
120
100
80
60
40
20
0
Age (ka)
ATL-1
ATL-2
ATL-4
OSL SAR
OSL SARA
VSL SAR
pIRIR290
IR50 corrected for fading
Average

Table 1: Fauna identified from the Atlit Railway Bridge site.

Species	**Cave II**	**Cave III**
Artiodactyla		
Bovidae cf. Aurochs (cf. *Bos primigenius*)		1 molar 1 hyoid frag.
Fallow deer (*Dama mesopotamica*)		1 L scapula neck
Gazelle cf. Mountain gazelle (cf. *Gazella gazella*)	1 metapodial shaft frag. 1 metapodial prox. frag.	1 R tibia prox. epiphysis 1 L tibia shaft & dist. epiphysis
Mammalia		
Large mammal	1 R humerus shaft – *Bos*/*Cervus* size undet. long bone shaft frag. 7 undet. long bone shaft frag.	
Medium mammal		3 undet. long bone shaft frags cf. Gazelle tibia
Aves		
cf. partridge (cf. *Alectoris chukar*)	1 R dist. tibiotarsus	
Ostrich (*Struthio camelus*)	1 eggshell frag.	
Reptilia		
Spur thighed tortoise (*Testudo graeca*)		1 R hypoplastron
Mollusca		
*Glycymeris nummaria**		2 valves & 3 frags.
Acanthocardia tuberculata		2 frags.
Cerastoderma glaucum		1 frags.
Donax trunculus		2 frags.

*previous name for this species was *Glycymeris insubrica*

Key: prox=proximal; dist= distal; L =left; R= right; undet= undetermined; frag.= fragment

Table 2: Luminescence dating field and laboratory data, dose rates and ages.

Lab code	Grain Size (µm)	K (%)	U (ppm)	Th (ppm)	Ext. α (µGy/a)	Ext. β (µGy/a)	Ext. γ (µGy/a)	Dose rate (µGy/a)	No. aliquots	OD (%)	De (Gy)	Fading (%/decade)	Age (Ka)
ATL-1 QZ OSL	**88-125**	**0.07**	**1.73**	**0.82**	**5**	**265**	**226**	**580±21**	**30**	**28**	**51.5±2.7**	**2.6±0.4**	**89±6**
ATL-1 QZ SARA									**24**		**54.6±6.6**		**94±11**
ATL-1 QZ VSL									**16**	**12**	**48.8±2.4**		**84±5**
ATL-1 KF IR_{50}	**125-210**				**100**	**266**		**1230±146**	**16**	**9**	**68.8±1.6**		**73±6***
ATL-1 KF IR_{290}									**16**	**6**	**118±2.1**		**96±5**
Average:													***87±9***
ATL-2 QZ OSL	**88-125**	**0.07**	**1.46**	**0.58**	**4**	**228**	**188**	**505±19**	**31**	**18**	**48.8±1.7**	**3.0±0.3**	**97±5**
ATL-2 QZ SARA									**24**		**49.7±9.9**		**99±20**
ATL-2 QZ VSL									**21**	**30**	**42.3±2.9**		**84±7**
ATL-2 KF IR_{50}	**125-210**				**83**	**229**		**1138±144**	**12**	**7**	**66.4±1.5**		**80±6***
ATL-2 KF IR_{290}									**12**	**7**	**110±2.3**		**97±5**
Average:													***91±9***
ATL-4 QZ OSL	**88-125**	**0.08**	**2.77**	**0.50**	**7**	**386**	**320**	**798±25**	**34**	**16**	**53.2±1.6**	**3.1±0.2**	**67±3**
ATL-4 QZ SARA									**24**		**66.9±0.8**		**84±3**
ATL-4 QZ VSL									**30**	**21**	**53.8±2.2**		**67±4**
ATL-4 KF IR_{50}	**125-210**				**149**	**388**		**1495±151**	**12**	**3**	**62.8±0.7**		**58±4***
ATL-4 KF IR_{290}									**12**	**8**	**115±2.7**		**77±4**

Average:													***71±10***

Notes: Internal beta dose rate for alkali feldspars was calculated using K-contents of 12±0.5% and an estimated a-value of 0.15±0.05, giving a value of 553±50 μGy/a for the specific grain size (not in Table). Cosmic dose rate was evaluated at 85 μGy/a from estimated burial depth of 8±1 m (not in Table). Moisture contents were estimated at 10±3 %. Aliquots used – the number of aliquots used for the average De out of those measured. OD- Overdispersion, a measure of scatter within the sample beyond that expected from analytical noise. De averages and errors were calculated using the central age model (Galbraith and Roberts 2012). * IR_{50} ages were corrected for fading using the measured rates.

Table 3: Luminescence dating measurement protocols.

	a. OSL	b. VSL	c. IRSL
1	Give a regen dose (for N dose = 0)	Give a regen dose (for N dose = 0)	Give a regen dose (for N dose = 0)
2	Preheat for 10 s @ 260°C	Preheat for 100 s @ 300°C	Preheat for 60 s @ 320°C
3	Measure OSL with LED for 40 s @ 125°C (Ln)	Measure OSL with LED for 100 s @ 125°C	Measure IRSL for 200 s @ 50°C
4	Give a test dose of ~10 Gy	Measure VSL for 100 s @ RT (Ln)	Measure IRSL for 200 s @ 290°C (Ln)
5	Preheat for 10 s @ 220°C	Give a test dose of ~50 Gy	Give a test dose of 32 Gy
6	Measure OSL with LED for 40 s @ 125°C (Tn)	Preheat for 100 s @ 290°C	Preheat for 60 s @ 320°C
7	Deplete remaining OSL for 100 s @ 280°C	Measure OSL with LED for 100 s @ 125°C	Measure IRSL for 200 s @ 50°C
8	Return to Step 1	Measure VSL for 100 s @ RT (Tn)	Measure IRSL for 200 s @ 290°C (Tn)
9		Deplete remaining VSL for 200 s @ 280°C	Deplete remaining IRSL for 200 s @ 325°C
10		Return to Step 1	Return to Step 1

Notes: OSL (optically stimulated luminescence) protocol modified from Wintle and Murray (2006); VSL (violet stimulated luminescence) modified from Jain et al. (2009); IRSL (infrared stimulated luminescence) protocol from Thiel et al. (2011), which includes both IR_{50} and $pIRIR_{290}$ (p stands for post). The signals used for constructing a dose response curve and calculating the De are shaded.